Isocyanide Adducts of Tri- and Tetravalent Uranium Metallocenes Supported by Tetra(isopropyl)cyclopentadienyl Ligands

Michael A. Boreen,[a,b] Oliver A. Groß,[c] Stephan Hohloch,[d,*] and John Arnold[a,b,*]

[a]*Department of Chemistry, University of California, Berkeley, California 94720, USA*
[b]*Chemical Sciences Division, Lawrence Berkeley National Laboratory, Berkeley, California 94720, USA*
[c]*Paderborn University, Warburger Straße 100, 33098 Paderborn, Germany*
[d]*University of Innsbruck, Faculty of Chemistry and Pharmacy, Institute of General, Inorganic and Theoretical Chemistry, Innrain 80-82, 6020 Innsbruck, Austria.*

*Email: arnold@berkeley.edu, stephan.hohloch@uibk.ac.at

Supporting Information

NMR Spectroscopy

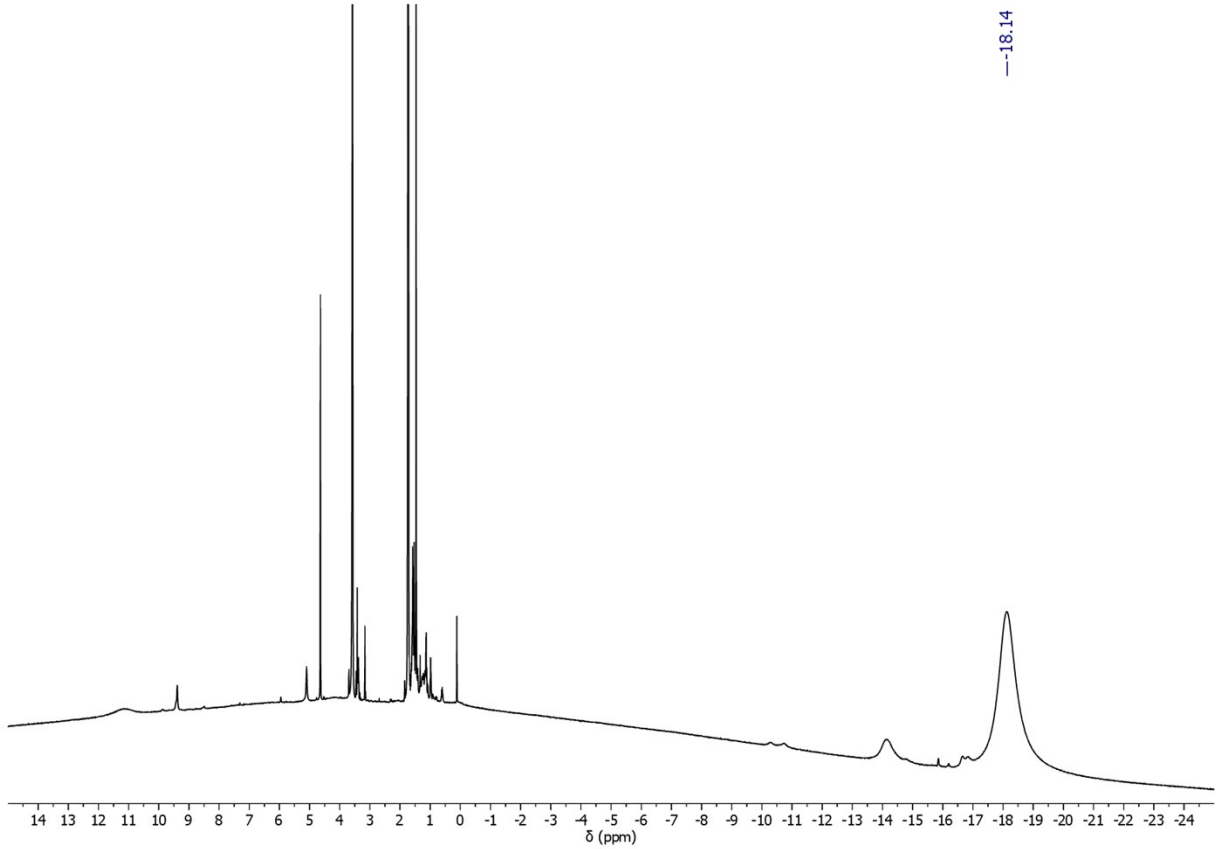

Figure S1. Room temperature 600 MHz ^{1}H NMR spectrum of **1** in THF-d_8. In **2** and **3**, the signals corresponding to the ^{t}Bu groups appear to be much sharper than those of the Cp^{iPr4} ligands, so the signal at −18.14 ppm is attributed to the ^{t}Bu protons of **1**. Given the broadness of this peak (FWHM = 400 Hz), the remaining resonances for the Cp^{iPr4} ligands of **1** are presumably too broad to be observed. The broad signal at −14.2 ppm was observed to increase in intensity after allowing the sample to sit at room temperature for 80 min, indicating that it corresponds to a decomposition product of **1**.

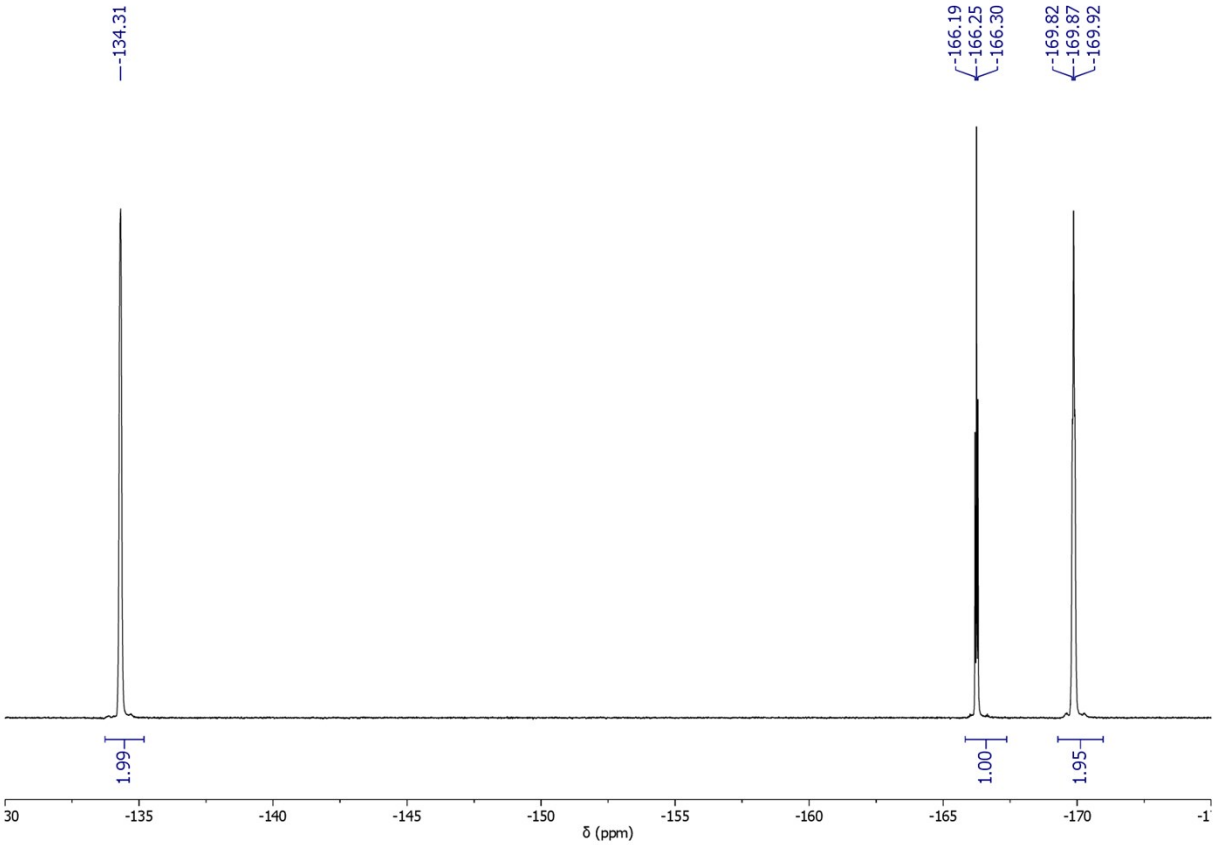

Figure S2. Room temperature 376 MHz ^{19}F NMR spectrum of **1** in THF-d_8.

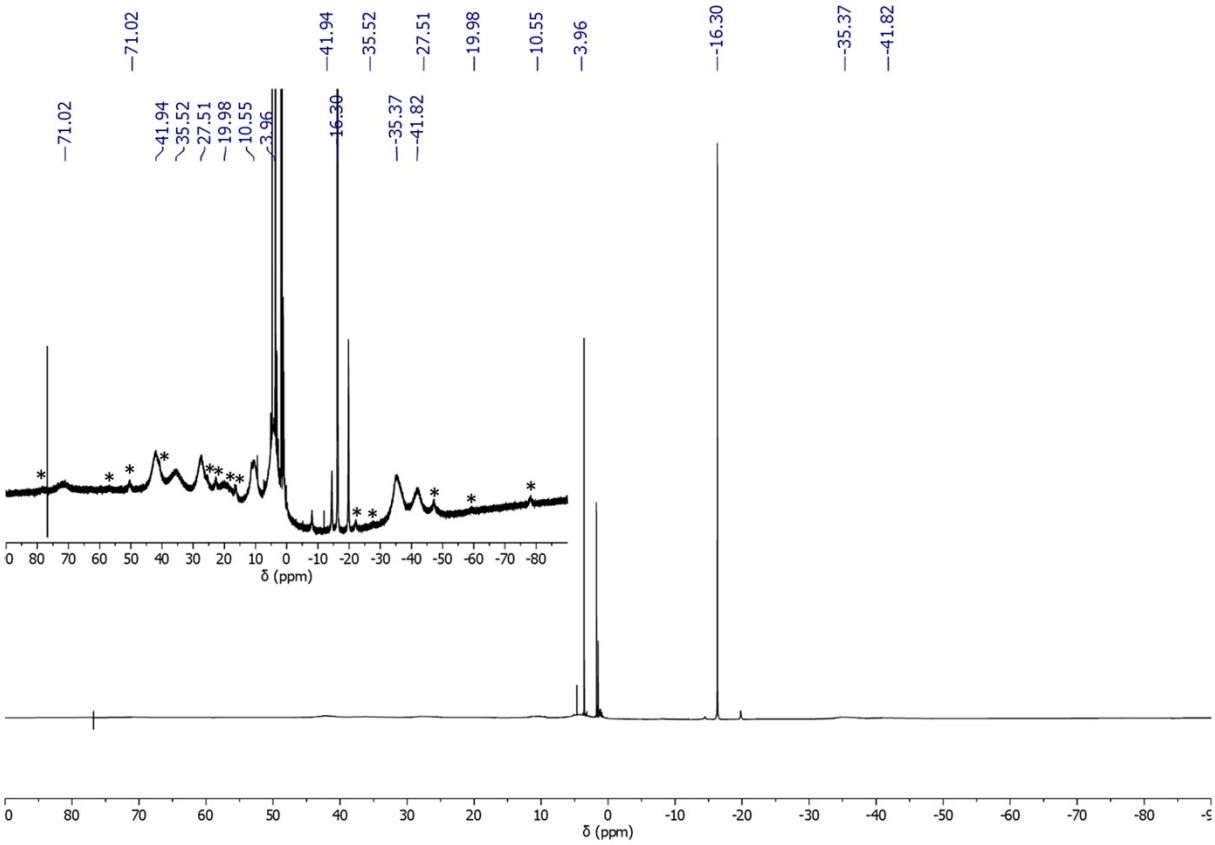

Figure S3. Room temperature 400 MHz ^{1}H NMR spectrum of **2** in THF-d_8. The inset spectrum is the same as the larger spectrum but with peak intensities increased. Due to the extreme broadness of the signals, it was not possible to correct the baseline of this spectrum. The chemical shift values shown are roughly centered on what appear to be individual broad signals corresponding to **2**, so their placement is tentative. Minor quantities of $(Cp^{iPr4})_2UI_2$ (*) were observed (as confirmed by spiking with an isolated sample of $(Cp^{iPr4})_2UI_2$) due to the considerably sharper nature of these resonances as compared to those of **2**.[1] The small but relatively sharp signals at −14.4 and −19.8 ppm could not be identified.

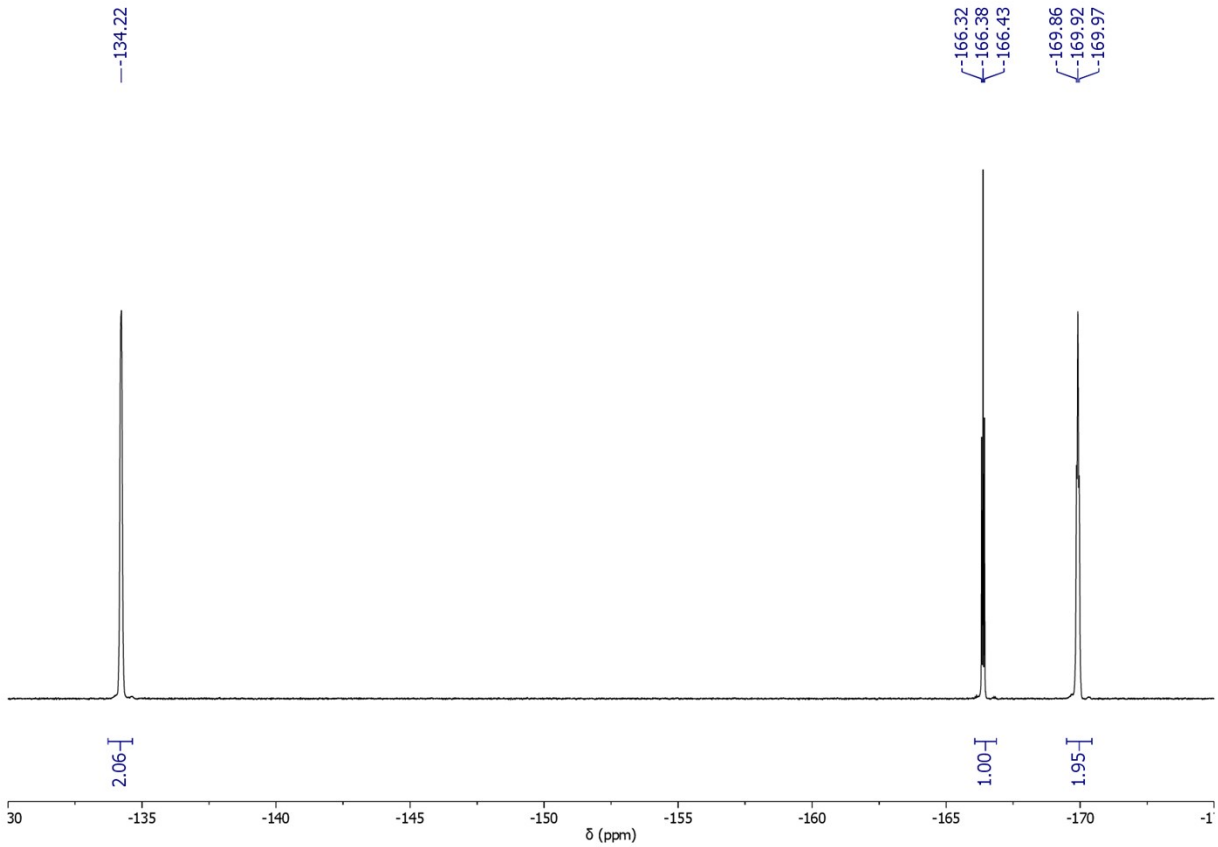

Figure S4. Room temperature 376 MHz ^{19}F NMR spectrum of **2** in THF-d_8.

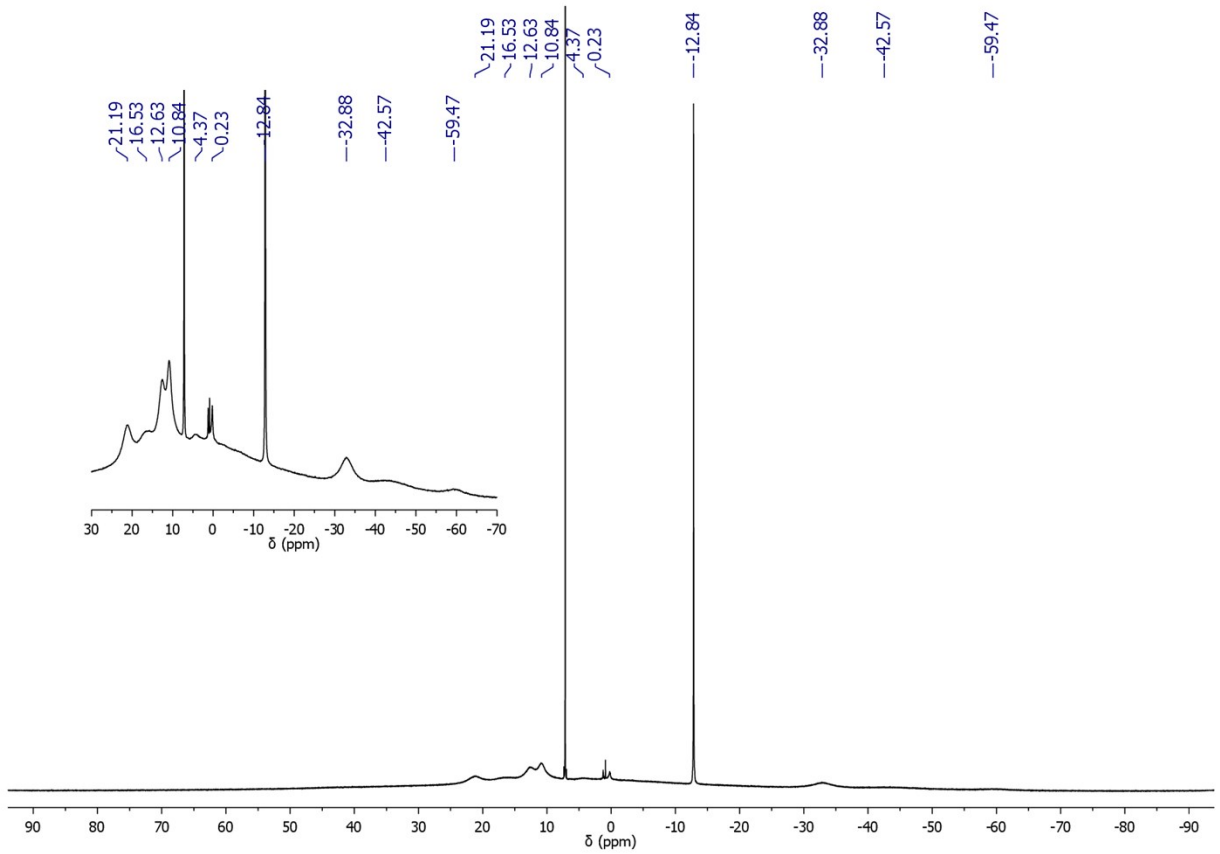

Figure S5. Room temperature 400 MHz ^{1}H NMR spectrum of **3** in C_6D_6. The inset spectrum has had a 10 Hz exponential line broadening function applied to improve the visibility of the broad peaks from the Cp^{iPr4} ligands.

UV-Visible Spectroscopy

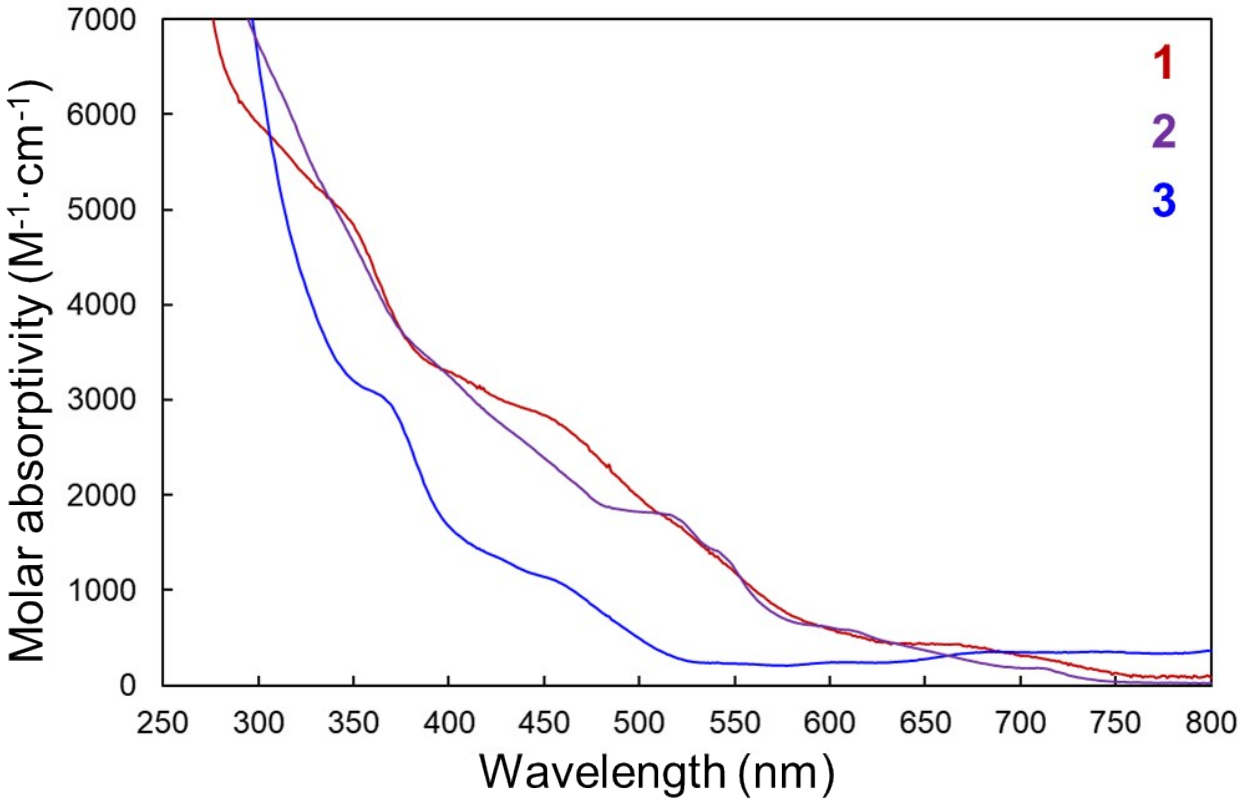

Figure S6. UV-visible spectra of **1**, **2**, and **3** in THF. The spectra of **1** and **2** are qualitatively similar to those of other uranium(IV) bis-Cp^{iPr4} complexes, and the spectrum of **3** is similar to that of $(Cp^{iPr4})_2UI$ in THF; $(Cp^{iPr4})_2UI$ coordinates THF in solution, presumably forming a $(Cp^{iPr4})_2U(I)(L)$ (L = neutral donor ligand) species similar to **3**.[1,2]

Details for GC/MS Analysis of Volatiles in Reaction Mixture to Form Complex 1

Hexane (1.5 mL) was added to a mixture of $(Cp^{iPr4})_2UI$ (18 mg, 0.022 mmol, 1.0 equiv) and $[(Et_3Si)_2(\mu\text{-H})][B(C_6F_5)_4]$ (20 mg, 0.022 mmol, 1.0 equiv), and the resulting suspension was stirred vigorously for 1 h at room temperature in a 20 mL scintillation vial. The solution was then decanted, and the blue solid was washed with 3 × 1 mL of hexane to remove any remaining Et_3SiI, Et_3SiH, and $(Cp^{iPr4})_2UI$. The crude $[(Cp^{iPr4})_2U][B(C_6F_5)_4]$ was extracted into 10 mL of diethyl ether and filtered through Celite; the resulting dark blue solution was transferred to a 25 mL Schlenk flask. A solution of ^{t}BuNC (10 µL, 0.090 mmol, 4.1 equiv) in 2 mL of diethyl ether was added to a separate 25 mL Schlenk tube. The ^{t}BuNC was added to the crude $[(Cp^{iPr4})_2U][B(C_6F_5)_4]$ solution by syringe at room temperature, and the resulting cloudy orange mixture was sealed and stirred for 20 min. The volatiles of the reaction mixture were then vacuum-transferred to a liquid nitrogen-cooled Schlenk tube. Once warmed to near room temperature, the flask was sealed until an aliquot was transferred to a separate vial for GC/MS analysis.

X-ray Crystallography

In a dry nitrogen glove box, samples of single crystals of **1**, **2**, and **3** were coated in Paratone-N oil prior to transport to diffraction facilities, where they were evaluated by polarized light microscopy and mounted on a Kaptan loop. X-ray diffraction data were collected at CheXray, Berkeley, CA, using a Bruker APEX II QUAZAR instrument outfitted with a monochromated radiation source (for **1** and **3**) or on a Rigaku XtaLAB P200 equipped with a MicroMax-007 HF microfocus rotating anode and a Pilatus 200K hybrid pixel array detector (for **2**); data for these samples were collected using Mo Kα radiation (λ = 0.71073 Å). All data collections were conducted at 100 K, with the crystals cooled by a stream of dry nitrogen. For **1** and **3**, Bruker APEX2 software was used for the data collections, Bruker SAINT V8.37A software was used to conduct the cell refinement and data reduction procedures,[3] and absorption corrections were carried out by a multi-scan method utilizing the SADABS program.[4] For **2**, CrysAlis^{Pro} was used for the data collections and data processing, including a multi-scan absorption correction applied using the SCALE3 ABSPACK scaling algorithm within CrysAlis^{Pro}.[5] Initial structure solutions were found using direct methods (SHELXT),[6] and refinements were carried out using SHELXL-2014.[7–9] Thermal parameters for all non-hydrogen atoms were refined anisotropically. All hydrogen atoms were placed at calculated positions and refined using a riding model. Thermal ellipsoid plots were made using Mercury.[10] Complex **1** possessed highly disordered outer sphere solvent molecules; the data for this structure were treated with the BYPASS routine included in the OLEX2 software package.[11] The final model for **1** contains a large Q-peak (6.76 e·Å^{-3}) near the uranium center attributed to minor unresolved twinning or disorder. Attempts to model a full set of secondary positions for the complex ion in **1** were unsuccessful, and attempts to model secondary positions for smaller fragments led to unreasonable structural metrics, so the model with the Q-peak unassigned was chosen as the most reasonable treatment of the data. All structures have been deposited to the Cambridge Crystallographic Data Centre (CCDC), with deposition numbers 2006480 (**1**), 2006481 (**2**), and 2006482 (**3**).

Table S1. Crystallographic data for $[(Cp^{iPr4})_2U(CN^tBu)_4][B(C_6F_5)_4]_2$ (**1**)

Empirical formula	$C_{102}H_{94}B_2F_{40}N_4U$	
Formula weight	2395.46	
Color, habit	Orange, plate	
Temperature	100(2) K	
Wavelength	0.71073 Å	
Crystal system	Triclinic	
Space group	P-1	
Unit cell dimensions	a = 13.9587(3) Å	α = 105.1690(10)°
	b = 13.9699(6) Å	β = 111.9920(10)°
	c = 16.9802(4) Å	γ = 95.6830(10)°
Volume	2890.56(16) $Å^3$	
Z / Z′	2 / 1	
Density (calculated)	1.376 Mg/m^3	
Absorption coefficient	1.511 mm^{-1}	
F(000)	1196.0	
Crystal size	0.20 × 0.08 × 0.02 mm^3	
Theta range for data collection	1.367 to 25.349°	
Index ranges	$-16 \le h \le 16$, $-16 \le k \le 16$, $-20 \le l \le 19$	
Reflections collected	32610	
Independent reflections	10440 [R_{int} = 0.0345]	
Completeness to theta = 25.242°	98.9%	
Absorption correction	Semi-empirical from equivalents	
Max. and min. transmission	0.4902 and 0.4300	
Refinement method	Full-matrix least-squares on F^2	
Data / restraints / parameters	10440 / 35 / 687	
Goodness-of-fit on F^2	1.063	
Final R indices [I > 2σ(I)]	R_1 = 0.0745, wR_2 = 0.1881	
R indices (all data)	R_1 = 0.0811, wR_2 = 0.1936	
Largest diff. peak and hole	6.76 and –0.94 $e \cdot Å^{-3}$	

Table S2. Crystallographic data for $[(Cp^{iPr4})_2U(I)(CN^tBu)_2][B(C_6F_5)_4]$ (**2**)

Empirical formula	$C_{68}H_{76}BF_{20}IN_2U$	
Formula weight	1677.04	
Color, habit	Red, block	
Temperature	100(2) K	
Wavelength	0.71073 Å	
Crystal system	Monoclinic	
Space group	$P2_1/c$	
Unit cell dimensions	a = 18.2004(4) Å	α = 90°
	b = 19.9489(3) Å	β = 111.882(2)°
	c = 19.6155(4) Å	γ = 90°
Volume	6608.8(2) $Å^3$	
Z	4	
Density (calculated)	1.685 Mg/m^3	
Absorption coefficient	3.022 mm^{-1}	
F(000)	3312.0	
Crystal size	0.27 × 0.19 × 0.12 mm^3	
Theta range for data collection	2.801 to 26.373°	
Index ranges	$-22 \le h \le 22$, $-21 \le k \le 24$, $-24 \le l \le 24$	
Reflections collected	78798	
Independent reflections	13508 [R_{int} = 0.0759]	
Completeness to theta = 25.242°	99.9%	
Absorption correction	Semi-empirical from equivalents	
Max. and min. transmission	1.00000 and 0.60464	
Refinement method	Full-matrix least-squares on F^2	
Data / restraints / parameters	13508 / 0 / 860	
Goodness-of-fit on F^2	1.053	
Final R indices [I > 2σ(I)]	R_1 = 0.0317, wR_2 = 0.0744	
R indices (all data)	R_1 = 0.0411, wR_2 = 0.0775	
Largest diff. peak and hole	1.24 and –1.64 $e \cdot Å^{-3}$	

Table S3. Crystallographic data for $(Cp^{iPr4})_2U(I)(CN^tBu)$ (**3**)

Empirical formula	$C_{39}H_{67}INU$	
Formula weight	914.86	
Color, habit	Green, plate	
Temperature	100(2) K	
Wavelength	0.71073 Å	
Crystal system	Triclinic	
Space group	P-1	
Unit cell dimensions	a = 10.3988(9) Å	α = 100.465(5)°
	b = 11.2181(11) Å	β = 96.791(5)°
	c = 18.702(2) Å	γ = 110.915(4)°
Volume	1963.8(4) $Å^3$	
Z	2	
Density (calculated)	1.547 Mg/m^3	
Absorption coefficient	4.943 mm^{-1}	
F(000)	906.0	
Crystal size	0.26 × 0.18 × 0.05 mm^3	
Theta range for data collection	2.003 to 25.350°	
Index ranges	$-10 \le h \le 12$, $-13 \le k \le 11$, $-22 \le l \le 21$	
Reflections collected	20926	
Independent reflections	7025 [R_{int} = 0.0481]	
Completeness to theta = 25.242°	97.7%	
Absorption correction	Semi-empirical from equivalents	
Max. and min. transmission	0.4901 and 0.3401	
Refinement method	Full-matrix least-squares on F^2	
Data / restraints / parameters	7025 / 18 / 398	
Goodness-of-fit on F^2	1.048	
Final R indices [I > 2σ(I)]	R_1 = 0.0452, wR_2 = 0.1108	
R indices (all data)	R_1 = 0.0613, wR_2 = 0.1209	
Largest diff. peak and hole	2.63 and –2.86 $e \cdot Å^{-3}$	

Electrochemistry

Cyclic voltammetry (CV) experiments were performed with a Gamry Reference 600™ potentiostat using screen-printed electrodes (SPEs) manufactured by Pine Research Instrumentation. The SPEs have platinum working and counter electrodes and a built-in silver pseudo-reference electrode. The electrodes are screen-printed onto a ceramic substrate such that the three electrodes are in close proximity to each other, without touching, at all times. The measurements were conducted in a dry N_2 atmosphere glovebox with 2–3 mM analyte in 0.2 M solutions of $[^{n}Bu_4N][B(C_6F_5)_4]$[12] in THF at room temperature. Potentials were referenced versus the ferrocene(Fc)/ferrocenium(Fc^+) redox couple by adding Fc (sublimed) as an internal standard for calibration at the end of each set of measurements.

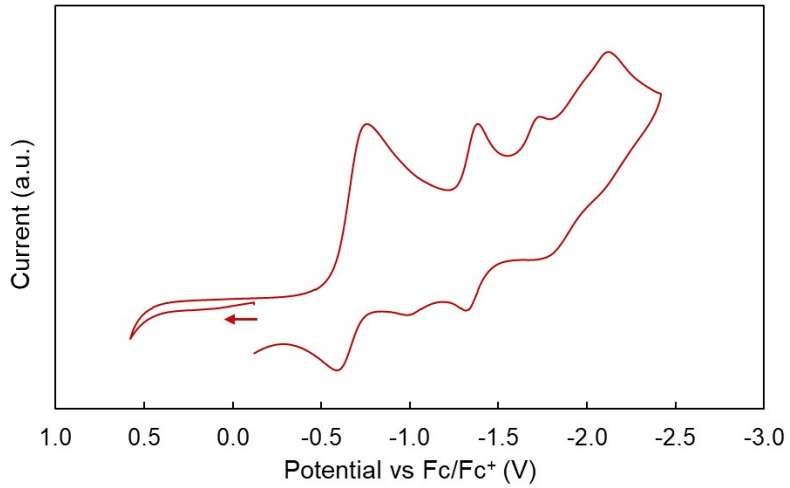

Figure S7. Cyclic voltammogram of $[(Cp^{iPr4})_2U(CN^{t}Bu)_4][B(C_6F_5)_4]_2$ (**1**) performed in THF with 0.2 M $[^{n}Bu_4N][B(C_6F_5)_4]$ electrolyte (scan rate = 100 mV/s). $E_{1/2}$ values of −0.68 and −1.35 V vs Fc/Fc^+ for the first and second reductive features, respectively, were measured. Notably, complex **1** decomposed completely within several minutes under these conditions.

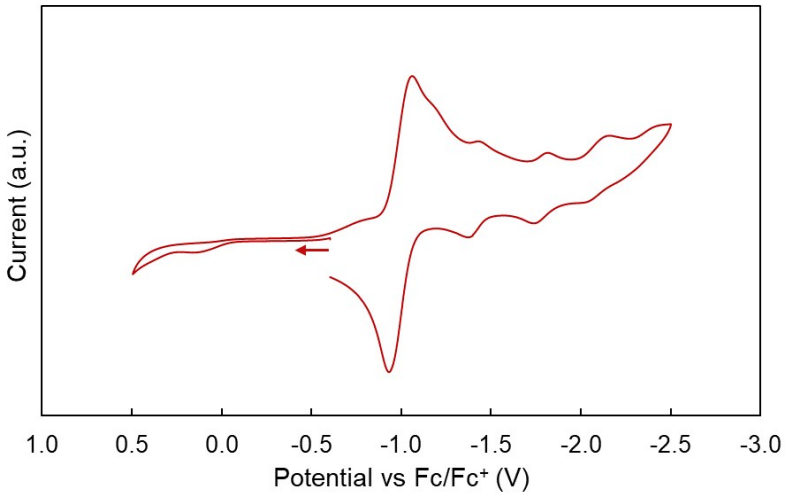

Figure S8. Cyclic voltammogram of $[(Cp^{iPr4})_2U(I)(CN^tBu)_2][B(C_6F_5)_4]$ (**2**) performed in THF with 0.2 M $[^nBu_4N][B(C_6F_5)_4]$ electrolyte (scan rate = 100 mV/s). An $E_{1/2}$ value of −1.00 V vs Fc/Fc^+ was measured for the first reductive feature. Notably, complex **1** decomposed significantly (not completely) within several minutes under these conditions.

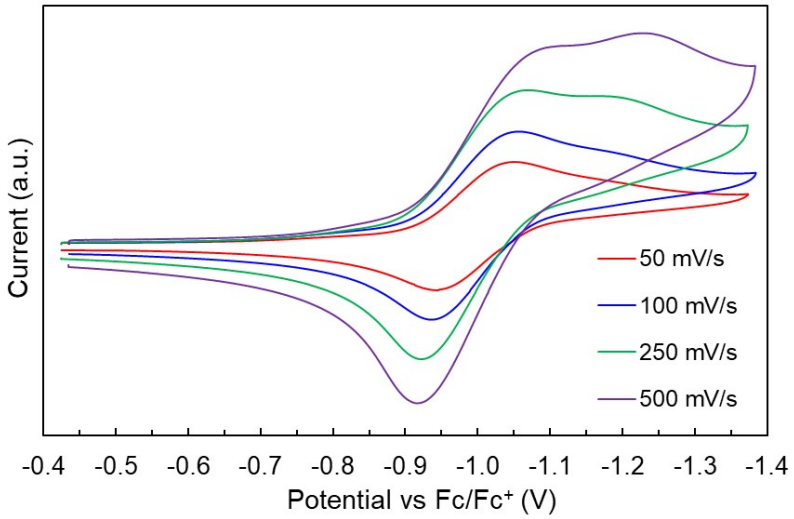

Figure S9. Scan rate-dependent measurements of the first reductive feature of **2**.

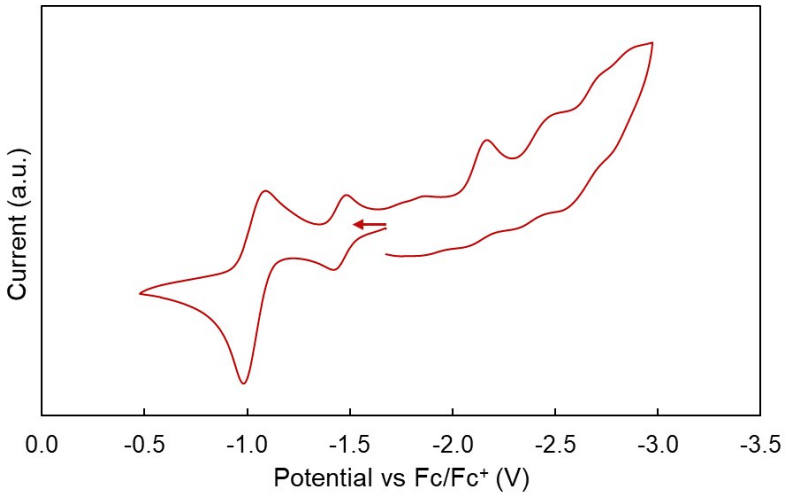

Figure S11. Cyclic voltammogram of $(Cp^{iPr4})_2U(I)(CN^tBu)$ (**3**) performed in THF with 0.2 M $[^nBu_4N][B(C_6F_5)_4]$ electrolyte (scan rate = 100 mV/s). $E_{1/2}$ values of −1.45 and −1.03 V vs Fc/Fc^+ for the first and second oxidative features, respectively, were measured. The first reductive feature displays E_{pc} = −2.16 V.

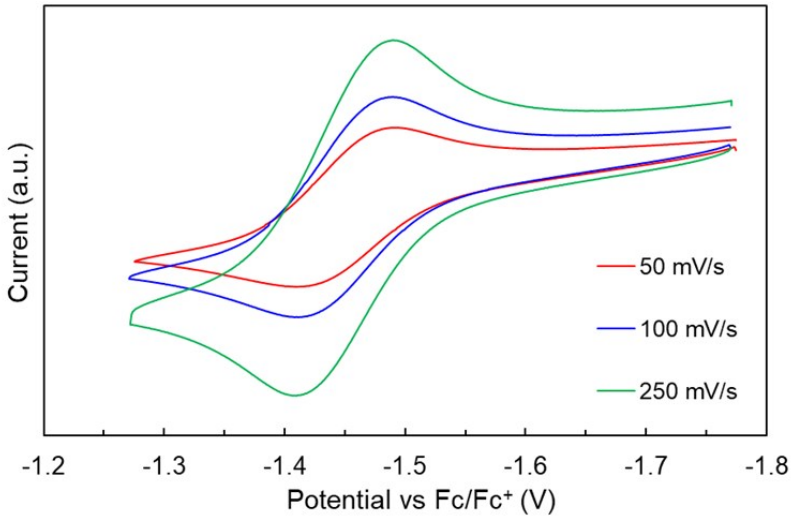

Figure S12. Scan rate-dependent measurements of the first oxidative feature of **3**.

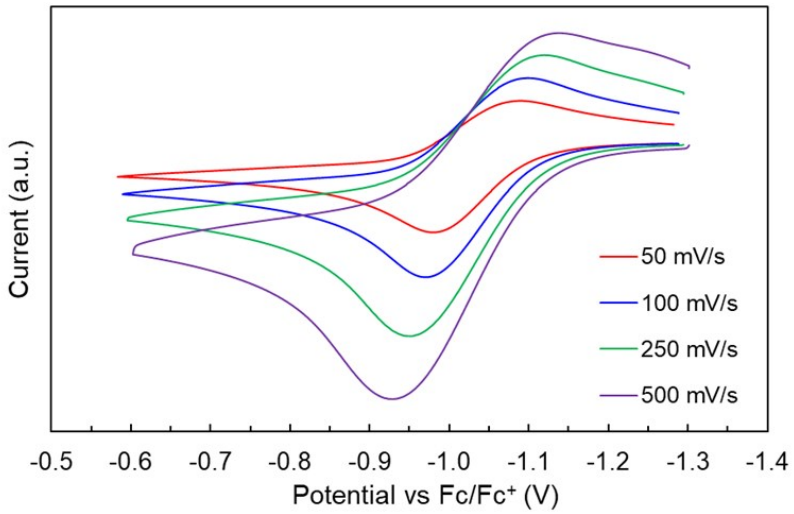

Figure S13. Scan rate-dependent measurements of the second oxidative feature of **3**.

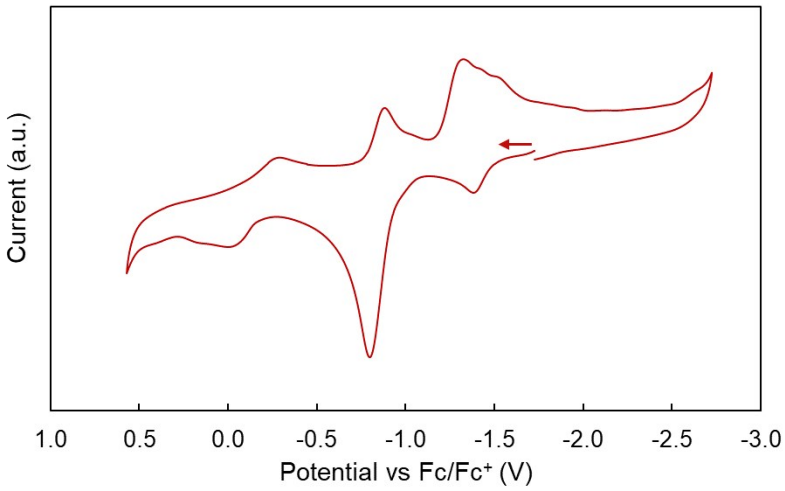

Figure S14. Cyclic voltammogram of $(Cp^{iPr4})_2UI$ performed in THF with 0.2 M $[^nBu_4N][B(C_6F_5)_4]$ electrolyte (scan rate = 100 mV/s). Note: $(Cp^{iPr4})_2UI$ has been shown previously to reversibly bind THF.[1] The first two oxidative features display two return waves. Furthermore, at higher scan rates, the return wave closer in potential to the oxidative wave became relatively more intense than the other return wave (see Figures S15–S17). Using the closer return waves, $E_{1/2}$ values of −1.41 and −0.84 V vs Fc/Fc^+ for the first and second oxidative features, respectively, were measured. The third oxidative feature displays E_{pa} = 0.00 V and E_{pc} = −0.29 V.

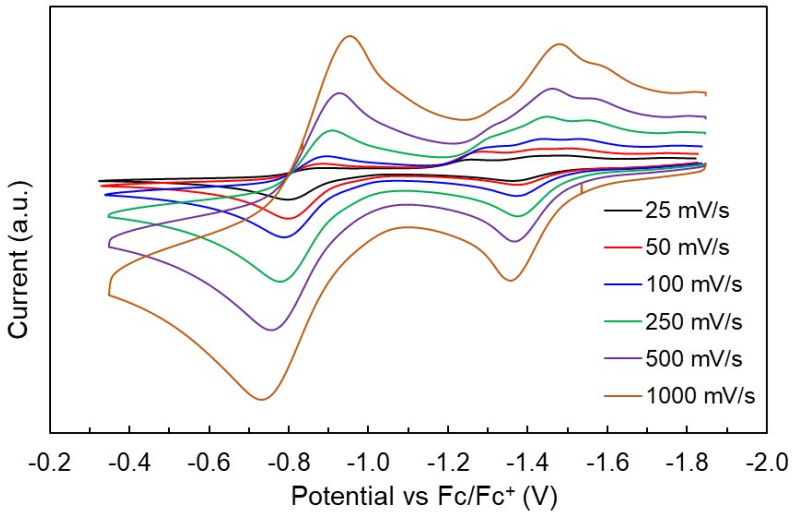

Figure S15. Scan rate-dependent measurements of the first two oxidative features of $(Cp^{iPr4})_2UI$.

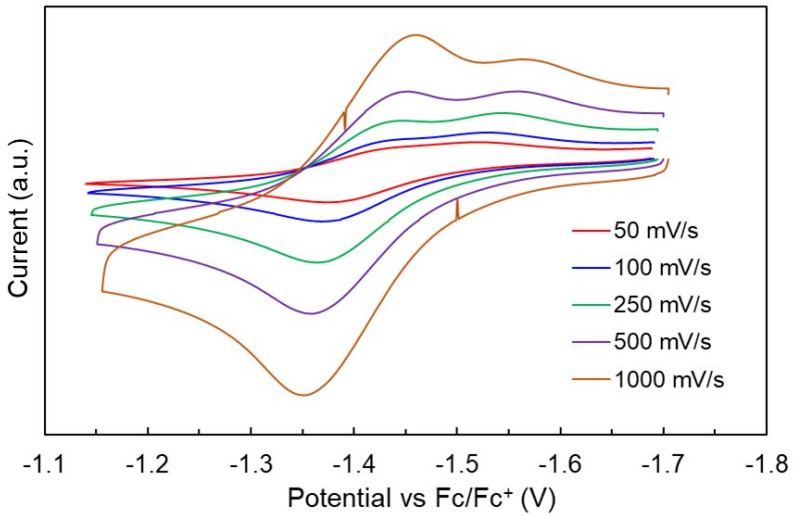

Figure S16. Scan rate-dependent measurements of the first oxidative feature of $(Cp^{iPr4})_2UI$.

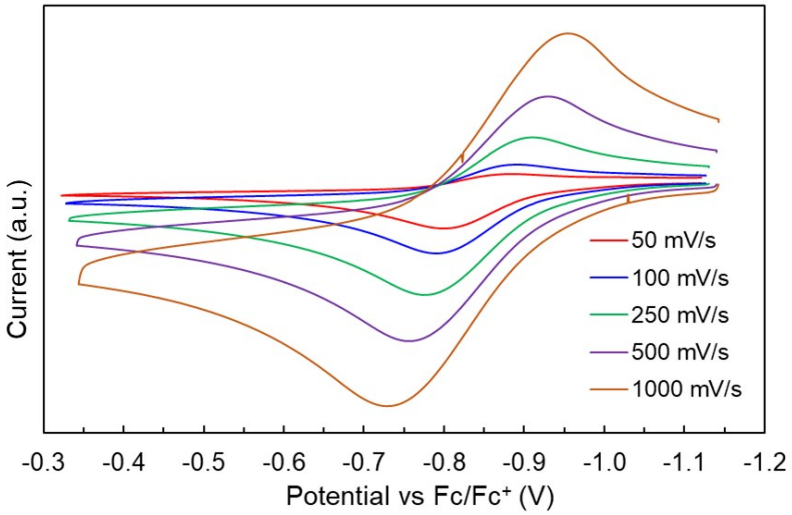

Figure S17. Scan rate-dependent measurements of the second oxidative feature of $(Cp^{iPr4})_2UI$.

References

(1) M. A. Boreen, D. J. Lussier, B. A. Skeel, T. D. Lohrey, F. A. Watt, D. K. Shuh, J. R. Long, S. Hohloch and J. Arnold, *Inorg. Chem.*, 2019, **58**, 16629.

(2) M. A. Boreen, K. N. McCabe, T. D. Lohrey, F. A. Watt, L. Maron, S. Hohloch and J. Arnold, *Inorg. Chem.*, 2020, **59**, 8580.

(3) Bruker, *APEX2, and SAINT*, Bruker AXS Inc., Madison, WI.

(4) Bruker, *SADABS*, Bruker AXS Inc., Madison, WI.

(5) Rigaku Oxford Diffraction, (2015), CrysAlisPro Software system, version 1.171.39.7a, Rigaku Corporation, Oxford, UK.

(6) G. M. Sheldrick, *Acta Crystallogr., Sect. A: Found. Adv.*, 2015, **71**, 3.

(7) G. M. Sheldrick, *Acta Crystallogr., Sect. A: Found. Adv.*, 2008, **64**, 112.

(8) O. V. Dolomanov, L. J. Bourhis, R. J. Gildea, J. A. K. Howard and H. Puschmann, *J. Appl. Crystallogr.*, 2009, **42**, 339.

(9) L. J. Farrugia, *J. Appl. Crystallogr.*, 2012, **45**, 849.

(10) C. F. Macrae, I. J. Bruno, J. A. Chisholm, P. R. Edgington, P. McCabe, E. Pidcock, L. Rodriguez-Monge, R. Taylor, J. Van De Streek and P. A. Wood, *J. Appl. Crystallogr.*, 2008, **41**, 466.

(11) P. Van Der Sluis and A. L. Spek, *Acta Crystallogr., Sect. A: Found. Adv.*, 1990, **46**, 194.

(12) E. J. Lawrence, V. S. Oganesyan, G. G. Wildgoose and A. E. Ashley, *Dalton Trans.* 2013, **42**, 782.